

Asteroseismology of red giants: photometric observations of Arcturus by *SMEI*

N. J. Tarrant, W. J. Chaplin, Y. Elsworth, S. A. Spreckley, I. R. Stevens

School of Physics and Astronomy, University of Birmingham, Edgbaston, Birmingham B15 2TT, U.K.

29 October 2018

ABSTRACT

We present new results on oscillations of the K1.5 III giant Arcturus (α Boo), from analysis of just over 2.5 yr of precise photometric observations made by the *Solar Mass Ejection Imager* (*SMEI*) on board the Coriolis satellite. A strong mode of oscillation is uncovered by the analysis, having frequency $3.51 \pm 0.03 \mu\text{Hz}$. By fitting its mode peak, we are able offer a highly constrained direct estimate of the damping time ($\tau = 24 \pm 1$ d). The data also hint at the possible presence of several radial-mode overtones, and maybe some non-radial modes. We are also able to measure the properties of the granulation on the star, with the characteristic timescale for the granulation estimated to be $\sim 0.50 \pm 0.05$ d.

Key words:

stars: individual (Arcturus) – stars: red giants – stars: oscillations

1 INTRODUCTION

Oscillations have now been observed in several G and K-class red giant stars (see Bedding & Kjeldsen 2006, and references therein). The oscillations appear to be Sun-like in nature (Frandsen et al. 2002; de Ridder et al. 2006; Barban et al. 2007), meaning they are self excited stochastically by convection. It had been thought that the radial acoustic (p) modes would dominate the oscillation spectra (Christensen-Dalsgaard, 2004). However, recent observations by Hekker et al. (2006) suggest non-radial modes may also be present in some giants.

In this paper we present new results on oscillations of the K1.5 III giant Arcturus (α Boo), from analysis of photometric observations made by the *Solar Mass Ejection Imager* (*SMEI*) on board the Coriolis satellite. Arcturus has been the subject of several observing campaigns that have studied its variability. Observations of Arcturus made from the ground in Doppler velocity (e.g., Innis et al. 1998; Belmonte et al. 1990; Hatzes & Cochran 1994; Merline 1995), and from space in photometric intensity (Retter et al. 2003), have uncovered evidence for variability on periods of the order of a few days. These periods correspond to frequencies of a few micro-Hertz, and are close to predictions for acoustic modes based on estimates of the mass, radius and effective temperature of Arcturus (see Section 2 below).

While Arcturus is, indisputably, a variable star, no studies to date have presented convincing evidence for the identification of *individual* modes of oscillation. This can be something of a non-trivial problem for red giants. First, spacings in frequency between radial overtones are expected to be small. This is because the spacings are predicted to scale, to first order, with the square root of the mean densities of the stars. The predicted spacing for

Arcturus, based on estimates of its mass and radius, is only $\approx 0.9 \mu\text{Hz}$. Such a small spacing places demands on the length of dataset required to resolve peaks cleanly in frequency. Second, if the damping of stochastically excited modes is sufficiently strong it can give peaks widths that may cause neighbouring modes to overlap in frequency (see Stello et al. 2006). Third, if non-radial modes are observed at prominent levels they will give rise to additional crowding of the mode spectrum. Some of these non-radial modes may be expected to possess mixed acoustic and gravity-mode-like characteristics. The spacings in frequency of these mixed modes can be somewhat irregular (Christensen-Dalsgaard, 2004) creating further complications for mode identification, particularly in short datasets, if they appear at observable levels.

The *SMEI* observations that we present here extend over a period lasting just over two-and-a-half years, and have a reasonable overall duty cycle. The excellent resolution possible in frequency is unprecedented for near-continuous, high-cadence photometric studies of red giant variability, and we are able to identify, for the first time, individual modes of oscillation of Arcturus. We offer a direct estimate of the mode damping time. And our results also hint at the possible presence of several radial-mode overtones, and maybe some non-radial modes. Finally, we are able to measure the granulation properties of the star.

2 DATA AND LIGHTCURVE EXTRACTION

The Coriolis satellite lies in a Sun-synchronous polar orbit of period ~ 101 minutes. *SMEI* comprises 3 cameras, each with a field of view of 60×3 degrees. The cameras are aligned such that the instantaneous total field of view is a strip of sky of size 170×3

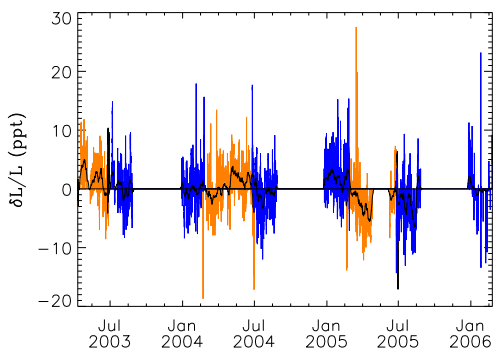


Figure 1. Residual lightcurves, in ppt, of the Camera #1 (orange) and Camera #2 (blue) data. The dark solid line shows the result of smoothing with a boxcar filter of width ~ 7 d.

degrees; a near-complete image of the sky is obtained from data on all three cameras after every orbit. Individual images – which are made from 10 stacked exposures, with a total integration time of about 40 sec – occupy an arc-shaped 1242×256 -pixel section of each 1272×576 -pixel CCD. Observations are made in white light, and the spectral response of the cameras is very broad, extending from ~ 500 to ~ 900 nm, with a peak at about 700 nm. A detailed description of the data analysis pipeline used to generate the lightcurves may be found in Spreckley & Stevens (in preparation). Here, we give a brief summary of the main steps.

Poor-quality frames having high background are first excluded from any further processing. Processing of the good frames begins with subtraction of bias, calculated from overscan regions at the edges of each frame, and a temperature-scaled dark-current signal. The frames are then flat fielded and spurious signals from cosmic ray hits are removed from the images. The Camera #2 data suffer from some stray light, and further cleaning of these data is performed to minimize the stray-light contribution (Buffington, private communication). The stray-light problem is concentrated in a small number of pixels on the CCD, and is not a major cause of concern for the data collected on Arcturus. Once the images have been cleaned aperture photometry is performed with a modified version of the *DAOPHOT* routines (Stetson 1987). The target star is tracked, and its lightcurve is corrected for the degradation of the CCD over the course of the mission, and a position-dependent correction is applied to compensate for variation of the Point Spread Function (PSF) across the frames. When the star lies within the field of view of one of the cameras, a single photometric measurement of its intensity is therefore obtained once every orbit.

We have obtained lightcurves of Arcturus from the Camera #1 and Camera #2 data. (There are some problems with data from Camera #3, which points closest to the Sun.) The Camera #1 lightcurve, which

begins 2003 April 10, comprises three data segments when Arcturus was visible, each having a length up to 120 days, with ~ 240 -day data gaps between each segment. Within each segment 50 to 70 per cent of data points are usable, with a fill of 25.6 per cent over the entire 812.2-day length. The Camera #2 lightcurve, which begins 2003 June 24, comprises six segments of observations each having a length around 60 days, separated by ~ 120 -day gaps. Apart from the shorter final segment, 60 to 80 per cent of the data points are usable in each segment, with a fill of 23.1 per cent over the entire 975.7-day length.

Fig. 1 shows the residual lightcurves of both cameras, in units of parts per thousand (ppt). The residual lightcurves for each camera were calculated, independently, as follows. The mean intensity was first computed for the usable data in all segments of a given camera. Fractional variations, $\delta L/L$, were then calculated with respect to this mean intensity. No adjustments were made to match the residuals from the two cameras. The Camera #1 lightcurve residuals are plotted in orange, and the Camera #2 residuals are plotted in blue. The dark solid line shows the result of smoothing with a boxcar filter of width ~ 7 d. The estimated point-to-point photometric precision of the observations made by both cameras, derived from the high-frequency noise, is ~ 1.5 ppt (see also Section 5 and Fig. 5). Note that we also created a combined dataset by concatenation of the residuals from the two cameras, resulting in a set with a combined length of 1051.4 days, and fill of 39.5 per cent.

The residual lightcurves show evidence of long-period variability, of amplitude several ppt, on timescales of a few hundred days. The plot demonstrates that observed trends appear to continue across transitions in coverage from one camera to another, suggesting they may well have a stellar component to them. It is interesting to note that the observed variations are similar, both in amplitude and timescale, to the long-period variations observed in Doppler velocity by Irwin et al. (1989), Hatzes & Cochran (1993) and Gray & Brown (2006). That said, there may be some instrumental contributions to the long-period trends. A detailed survey on the long-period stability of the *SMEI* photometric data is currently the subject of ongoing work (Spreckley & Stevens, in preparation).

Power density spectra of the Camera #1 and #2 residual lightcurves are shown in Fig. 2 between 0 to $30\mu\text{Hz}$. The raw spectra are rendered in grey. The red lines show the results of smoothing each spectrum with a boxcar filter of width $\sim 0.7\mu\text{Hz}$. The blue lines show power law fits to the background (see Section 3). The insets to both panels show power spectra of the window functions. (The window spectra are dominated by the effects of the 360 and 180-day gaps between the start times of data segments in each lightcurve, giving peaks at separations of 0.03 and $0.06\mu\text{Hz}$, respectively.)

The power density spectra of both residual lightcurves show concentrations of power, centered on about $4\mu\text{Hz}$, which appear to lie above the slowly varying background. A prominent peak located at $\approx 3.5\mu\text{Hz}$ in the Camera #2 spectrum is particularly striking ($S/N \approx 8$ in power). The locations in frequency of these peaks are consistent with predictions for p modes based on simple scaling relations that work well for Main Sequence, subgiant and giant stars. Bedding & Kjeldsen (2003) have shown that the frequency at which Sun-like oscillations have their maximum observed amplitudes scales with the acoustic cut-off frequency, i.e., as $\sim MR^{-2}T_{\text{eff}}^{-1/2}$. The radius and effective temperature of Arcturus are both well determined, e.g., $R = 25.4 \pm 0.3 R_{\odot}$ (Gray & Brown 2006) and $T_{\text{eff}} = 4290 \pm 30$ K (Griffin & Lynas-Grey 1999). The mass is less well constrained. Taking $M = 0.8 \pm 0.3 M_{\odot}$ (Bonnell & Bell 1993), and scaling against the frequency of maximum power for radial solar p modes of $3100\mu\text{Hz}$, the prediction is that the maximum of the Arcturus p-mode spectrum should lie at $\sim 4.5 \pm 1.7\mu\text{Hz}$.

The power in the peaks, in particular that in the $\approx 3.5\mu\text{Hz}$ peak, is also consistent with the excess power observed by Retter et al. (2003) in photometric observations of Arcturus lasting 19 d, which were made by the *Wide Field Infrared Explorer* (*WIRE*) satellite. Retter et al. attributed this excess power as being due to either several p modes, or a single, more heavily damped p mode. Because the *SMEI* lightcurves are much longer than the *WIRE* lightcurve, giving superior resolution in frequency, we are in a bet-

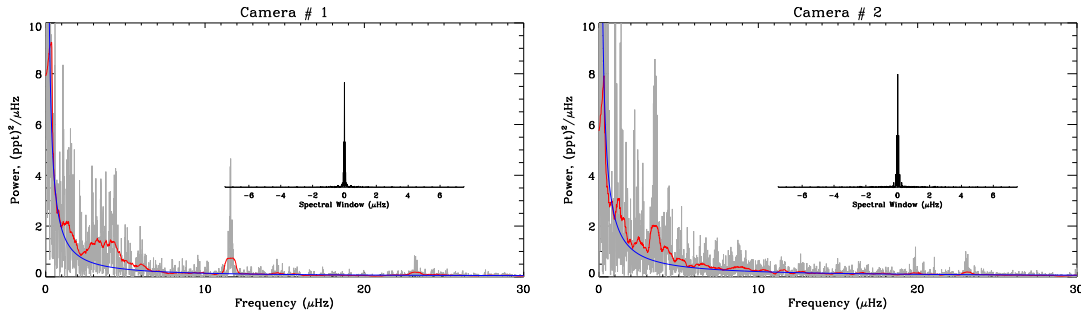


Figure 2. Power density spectra of the Camera #1 (left-hand panel) and Camera #2 (right-hand panel) residual lightcurves. The spectra are rendered in grey. Smoothed power spectra are shown as red lines. The blue lines show power law fits to the background (see Section 3). The insets show spectral windows for each dataset, at the same horizontal frequency scale as the main plots.

ter position to determine the nature of the excess power. We discuss the characteristics of the *SMEI* peaks, and possible interpretations, below.

Before that, we note that the Camera #1 spectrum has a very prominent peak at the diurnal frequency of $11.57\text{ }\mu\text{Hz}$. Moreover, prominent harmonics of the diurnal frequency are present at other frequencies in the Camera #1 spectrum (e.g., the second harmonic at $\sim 23.1\text{ }\mu\text{Hz}$). A few overtones of the diurnal frequency are also present in the Camera #2 spectrum, though typically at far less significant levels. The peaks in both spectra come from weak signatures of stray earthlight in the data (there are much weaker diurnal signatures in the Camera #1 and #2 window functions). There also appears to be a second lump of power between $1 - 2\text{ }\mu\text{Hz}$. However, because of the sharply increasing background over this region these features are not statistically significant (the statistical tests are described below in Section 3).

3 ANALYSIS OF THE POWER DENSITY SPECTRA

Fig. 3 shows the region of interest in power density spectra of the Camera #1, Camera #2 and concatenated residual lightcurves, between 2 and $7\text{ }\mu\text{Hz}$. The raw spectra are again rendered in grey. The dark solid lines show the results of smoothing each spectrum with a boxcar filter of width $\sim 0.14\text{ }\mu\text{Hz}$.

The hashed regions in Fig. 3 have been added to guide the eye to locations where peaks appear to be present at the same frequencies in the spectra. Peaks marked by the forward-slanted blue hashes are located at ~ 3.5 , ~ 4.35 and $\sim 5.15\text{ }\mu\text{Hz}$ and show an approximate equidistant spacing in frequency (see Section 4 below). Both spectra also show a peak at $\sim 4.05\text{ }\mu\text{Hz}$ (backward-slanted red hashes) which does not respect the near equidistant spacing between the other peaks. Each spectrum also shows some other peaks in the range 2 to $3.2\text{ }\mu\text{Hz}$ which do not coincide in frequency.

It is certainly tempting to identify the peaks marked by the forward-slanted blue hashes as constituting a spectrum of overtones of radial p modes. But is each of the peaks significant, i.e., could the appearance of the spectra be replicated merely by the random fluctuations of a non-resonant, broad-band background? We tested the likelihood that either prominent spikes – a spike being a prominent power spectral density, or height, in a *single* frequency bin – or several prominent spikes lying in close proximity in frequency – i.e., peaks, which could be the signature of a damped mode – were part of the slowly rising (in frequency), smooth background noise. Our tests returned estimates of the probability of finding spikes or peaks by chance anywhere in the spectrum (from zero frequency up

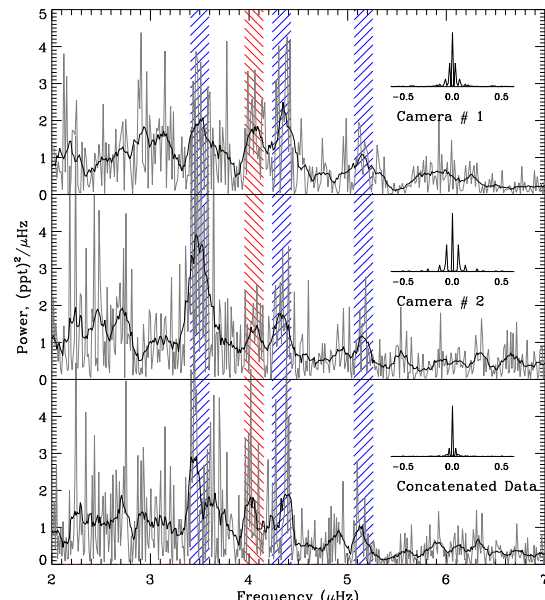


Figure 3. Power density spectra of the Camera #1 (upper plot) and Camera #2 (middle plot) and concatenated (lower plot) residual lightcurves, between 2 and $7\text{ }\mu\text{Hz}$. The insets show spectral windows for each dataset.

to the putative Nyquist frequency of $\sim 82.5\text{ }\mu\text{Hz}$). Low values of the returned probabilities would flag spikes or peaks as being deserving of further consideration as possible candidate modes. This is the so-called null, or H_0 , hypothesis. We refer the reader to Chaplin et al. (2002) and Appourchaux (2004) for full details on the spike and peak tests.

Our tests demanded that we pre-whiten the spectra first to allow us to determine heights of peaks relative to the local background levels, which of course change with frequency. We obtained estimates of the underlying backgrounds in two different ways, both of which involved fitting models to the observed power density spectra: (i) by fits of a simple power law $P(\nu) = a\nu^b + c$, where a , b and c were coefficients to be fitted; and (ii) by fits of a three-component model, including a component to represent explicitly granulation, which is described more fully in Section 5 below. The smooth background estimates given by fitting model (i) to each spectrum are shown as blue lines in each panel of Fig. 2.

In order to give robust estimates of the likelihood of spikes and peaks occurring by chance we used Monte Carlo simulations of artificial data, modulated by the window functions, to fix the

likelihood levels. In this way we were able to take proper account of the influence of windows upon results. Full details on the Monte Carlo simulations will be given in an upcoming paper. Here, we note that we created one thousand independent artificial realizations of the lightcurves for the two different models of the background described in the previous paragraph, each of which contained *no* artificial p modes. These data gave power density spectra closely resembling the observed spectra. By searching each of the artificial spectra for prominent spikes and peaks, using the methods applied to the real spectra, we were able to estimate likelihood distributions for our tests, and to therefore assign significance levels to each of the peaks in the real spectra.

We chose to flag as potential candidate modes those peaks which, when tested, had estimated likelihoods of ≤ 1 per cent of appearing by chance anywhere in the spectrum. In demanding that tests return such low likelihoods we sought to guard against possible false detections. (See Broomhall et al. 2007 for more discussion on fixing the threshold.) The peak at $\approx 3.5\,\mu\text{Hz}$ passed the significance threshold in the Camera #2 and concatenated datasets. We note that the peaks at ~ 3.5 , ~ 4.05 and $\sim 4.35\,\mu\text{Hz}$ did reach the ≈ 1 per cent level in certain tests in all spectra, but the likelihoods were notably less significant in other tests (with results depending on how the data were pre-whitened).

In summary, we conclude it is extremely unlikely that the Camera #2 peak at $3.5\,\mu\text{Hz}$ is due to noise. We feel confident in identifying this peak as being the signature of a mode. The other peaks in the range 2 to $7\,\mu\text{Hz}$ are certainly worthy of note, and may be the signatures of other modes; however, we cannot rule out, with the same degree of confidence, that they are not simply part of the background noise. That peaks appear at similar frequencies in the Camera #1 and #2 spectra is intriguing. It is of course possible to test the likelihood that peaks appear by chance in the same bin, or bins, of either spectrum (Broomhall et al. 2007) (having first truncated the Camera #2 lightcurve to be the same length as the Camera #1 lightcurve). Since the data in the lightcurves are almost completely independent in time, it is a trivial matter to find the joint likelihood of occurrence. When we tested against the joint likelihoods, the conclusions drawn from the independent tests were upheld.

4 DISCUSSION: PEAKS AS MODES

Our results in Section 3 above suggest it is likely that the prominent peak located in the Camera #2 spectrum at $3.5\,\mu\text{Hz}$ is the signature of a mode. What are the basic parameters of this mode? We have fitted the spectrum in the immediate vicinity of the mode to a multi-component model comprised of a resonant profile, to describe its peak, and a multi-component background. The obvious choice for the resonant profile is a Lorentzian function. However, if the Q -factor of the oscillation peak (i.e., frequency over linewidth, ν/Δ) is low, the full classical resonant function, which has terms in ν^4 , must be used. Here, the Q factor is a fairly modest ≈ 25 , and we tried both functions. The fitting model was also convolved with the Fourier transform of the window function to allow for redistribution of power by the window (see Fletcher 2007 for an in-depth discussion of the technique). Fits with either resonant profile gave very similar best-fitting parameters for the mode. We show the best fit to the peak, which incorporated the full classical function, in Fig. 4. The best-fitting mode parameters are also shown on the figure.

The results on this mode allow us to make several important remarks. The excellent frequency resolution of the data has allowed

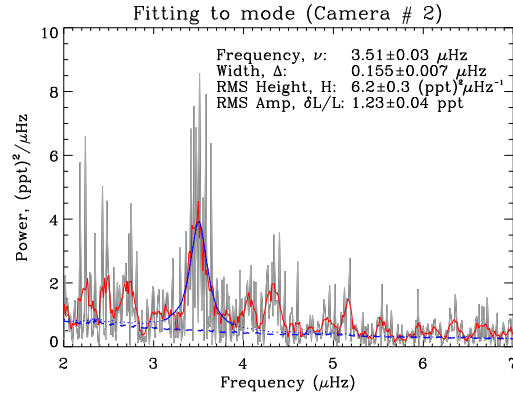


Figure 4. Fit to the mode seen in the Camera #2 power density spectrum. The raw spectrum is shown in grey and a 5-bin boxcar-smoothed spectrum in red. The best-fitting model is plotted in blue (with the solid part showing the range over which the mode was fitted); the background is plotted as the thick dashed line.

us to make a direct measurement of the width, Δ , of the mode, whose value implies a lifetime $\tau = 1/(\pi\Delta)$ of 24 ± 1 d. The presence of significant width, even after allowing for aliasing of power by the window function, implies the mode is stable, and excited stochastically by convection. The Q -factor of the mode peak is 23 ± 1 . This is slightly lower than the Q of ≈ 50 found for modes on the red giant ξ Hya (Stello et al. 2006); and similar to the Q of modes on the red giant ϵ Oph (Barban et al. 2007) [Q of ~ 30 , determined to a fractional precision of about 25 per cent].

Assuming the $3.5\,\mu\text{Hz}$ peak to be the strongest mode in the spectrum, the observed RMS amplitude is found to be in approximate agreement with the predicted amplitude given by the scaling relation of Kjeldsen & Bedding (1995). This relation uses the maximum amplitude of radial solar p modes as a baseline calibration, and gives amplitudes that scale linearly with the luminosity to mass ratio, L/M . There is also a correction for the colour of the star (i.e., T_{eff}) and the wavelength, λ , at which the observations are made. Taking the values given in Section 2 for T_{eff} , M and R , together with $\lambda = 700\,\text{nm}$, this being at the peak in sensitivity of the SMEI data, we obtain a predicted maximum RMS amplitude for Arcturus of $(dL/L) = 1.1 \pm 0.5$ ppt. This prediction agrees within errors with our observed amplitude. Samadi et al. (2007) have recently discussed how theoretical predictions for the amplitudes of Sun-like p modes are affected by the description of the dynamic properties of the turbulent convection. In one scenario, which Samadi et al. favour, the amplitudes are found to scale like $(L/M)^{0.7}$. Such a scaling would instead imply $(dL/L) = 0.2 \pm 0.1$ ppt for Arcturus. This prediction differs significantly from our observed RMS amplitude.

In order to provide further support for the conclusions given above, we also conducted simulations like those outlined in Section 3 but now with an artificial p mode included in each artificial dataset, having the same parameters as our best fit shown in Fig. 4. We were thereby able to verify that changes to the prominence and appearance of the $3.5\text{-}\mu\text{Hz}$ peak in the Camera #1, Camera #2 and concatenated residual lightcurve spectra, and the spectra of individual segments from each camera, were consistent with our inferred values for the mode lifetime, amplitude and S/N.

What of the other peaks in Fig. 3? Those peaks marked by the forward-slanted blue hashes show an equidistant spacing in frequency, of just over $\sim 0.8\,\mu\text{Hz}$. Taking the values given in Section 2 for M and R , and scaling against the mean observed spacing

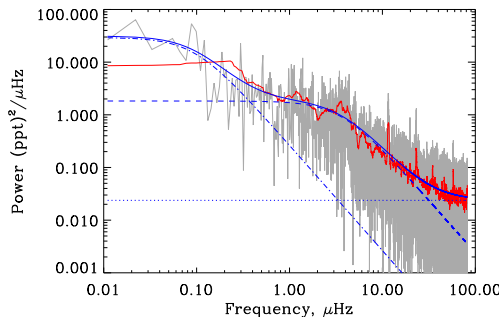


Figure 5. Power density spectrum of the concatenated residual lightcurve (smoothed in red), showing three-component model fit to the background. The overall best-fitting curve is plotted as a dark blue line, with contributions of individual components plotted as follows: photon shot noise (dotted lines); granulation (dashed lines); long-period noise, including stellar active-region noise, plus instrumental noise (dot-dashed line).

for radial solar p modes (of $135\,\mu\text{Hz}$), we get a predicted overtone spacing for Arcturus of $\sim 0.9\,\mu\text{Hz}$. So, one possible explanation for these peaks is that they correspond to three overtones of the fundamental radial mode. However, we remind the reader that we feel we cannot rule out, at least at a confidence level ≤ 1 per cent, that the peaks are not due to noise. Finally, we note the peak at $\sim 4.05\,\mu\text{Hz}$ marked by the backward-slanted red hashes in both spectra in Fig. 3. Could it be the signature of a non-radial mode? Again, we advise caution in over interpreting these results, but hope that improvements to the lightcurve pipeline may give cleaner data, and a more definitive answer regarding the origins of this peak, and the other peaks discussed above.

5 ESTIMATION OF GRANULATION PARAMETERS

Fig. 5 shows the power density spectrum of the concatenated residual lightcurve, with power now plotted on a logarithmic scale. The smooth dark blue line is the best-fitting curve of a three-component model used to describe the background power. The model contains a flat (white) component to describe the photon shot noise; and two power-law components to represent the contributions of granulation and stellar active region noise. It is important to remember that some of the long-period variability in the lightcurves (Fig. 1) may have an instrumental origin, and, as such, the third component must also take account of instrumental contributions. The second and third components were each described by the power-law model of Harvey (1985) (see also Bruntt et al. 2005). The Harvey model is specified by two parameters: a standard deviation, σ , and a characteristic timescale, τ . The best-fitting power contributions of the individual components are plotted as dotted (shot noise), dashed (granulation noise) and dot-dashed (long-period noise) lines in Fig. 5. The unprecedented frequency resolution allows well-constrained estimates of the granulation parameters to be extracted. The characteristic ‘knee’ in the power spectral density, which is given by the flattening of the granulation power at low frequencies, is clearly apparent in the spectrum (see region near $\approx 1\,\mu\text{Hz}$). The Camera #1 and #2 spectra show the same feature, and are of similar appearance to Fig. 5. The best-fitting granulation parameters for the spectrum of the concatenated residual lightcurve are: $\sigma = 4.56 \pm 0.06\,\text{ppt}$ and $\tau = 0.502 \pm 0.004\,\text{days}$. Comparison of the σ and τ values from similar fits to each of the Camera #1 and #2

spectra gives a guide to the actual external precision in the parameters: ≈ 10 per cent in σ , and ≈ 10 per cent in τ .

6 CONCLUSION

From our analysis of photometric observations made by *SMEI*, we have identified a prominent mode of oscillation on Arcturus (see parameters listed in Fig. 4) and, by fitting its resonant peak, have obtained a precise estimate of its damping time ($\tau = 24 \pm 1\,\text{d}$). The excellent resolution in frequency is unprecedented for near-continuous, high-cadence photometric studies of red giant variability, and this is the first time an individual mode of oscillation of Arcturus has been identified unambiguously. Analysis also hints at the possible presence of several radial-mode overtones, and maybe some non-radial modes, at frequencies in the range ≈ 2 to $5.5\,\mu\text{Hz}$. We have also measured the granulation properties of the star.

ACKNOWLEDGMENTS

NJT and SAS acknowledge the support of STFC. SAS also acknowledges the support of the School of Physics & Astronomy, University of Birmingham. *SMEI* was designed and constructed by a team of scientists and engineers from the US Air Force Research Laboratory, the University of California at San Diego, Boston College, Boston University, and the University of Birmingham. We single out A. Buffington, C. J. Eyles and S. J. Tappin for particular thanks. We also thank the referee for helpful comments.

REFERENCES

- Appourchaux T., 2004, A&A, 428, 1039
- Barban C., et al., 2007, A&A, 468, 1033
- Bedding T. R., Kjeldsen H., 2003, PASA, 20, 203
- Bedding T. R., Kjeldsen H., 2006, in: SOHO18/GONG 2006/HELAS I, ‘Beyond the spherical Sun’, August 2006, Sheffield, ed. M. Thompson, ESA SP-624, Noordwijk, Netherlands, p. 25.1
- Belmonte J. A., Jones A. R., Pallé P., Roca-Cortés T., 1990, ApJ, 358, 595
- Bonnell, J. T., Bell, R. A., 1993, MNRAS, 264, 334
- Broomhall A.-M., Chaplin W. J., Elsworth Y., Appourchaux T., 2007, MNRAS, 379, 2
- Bruntt H., Kjeldsen H., Buzasi D. L., Bedding T. R., 2005, ApJ, 633, 440
- Chaplin W. J., et al., 2002, MNRAS, 336, 979
- Christensen-Dalsgaard J., 2004, Sol. Phys., 220, 137
- de Ridder J., et al., 2006, A&A, 448, 689
- Fletcher S. T., 2007, PhD thesis, University of Birmingham, UK
- Frandsen S., et al., 2002, A&A, 394, 5
- Gray D. F., Brown K. I. T., 2006, PASP, 118, 1112
- Griffin R. E. M., Lynas-Grey A. E., 1999, AJ, 117, 2998
- Harvey J., 1985, in: Future missions in solar, heliospheric and space plasma physics, eds. E. Rolfe, B. Battrick, ESA SP-235, Noordwijk, Netherlands, p. 199
- Hatzen A. P., Cochran W. D., 1993, ApJ, 413, 339
- Hatzen A. P., Cochran W. D., 1994, ApJ, 422, 366
- Hekker S., Aerts C., de Ridder J., Carrier F., 2006, A&A, 458, 931
- Innis J. L., et al., 1998, in: Seismology of the Sun and Sun-like Stars, eds. V. Domingo, E. J. Rolfe, ESA SP-286, Noordwijk, Netherlands, p. 569
- Irwin A. W., Campbell B., Morbey C. L., Walker G. A. H., Yang S., 1989, PASP, 101, 147
- Kjeldsen H., Bedding T. R., 1995, A&A, 293, 87
- Merline W. J., 1995, PhD thesis, Univ. Arizona
- Retter A., Bedding T. R., Buzasi D. L., Kjeldsen H., Kiss L. L., 2003, ApJ, 591, L151

Samadi R., Georgobiani D., Trampedach R., Goupil M. J., Stein R. F., Nordlund A., 2007, A&A, 463, 297
Stello D., Kjeldsen H., Bedding T. R., Buzasi D., 2006, A&A, 448, 709
Stetson P. B., 1987, PASP, 99, 191